Journal of Biomedical Optics

SPIEDigitalLibrary.org/jbo

Time-resolved study of the mechanical response of tissue phantoms to nanosecond laser pulses

Francisco G. Pérez-Gutiérrez
Santiago Camacho-López
Guillermo Aguilar

SPIE

Time-resolved study of the mechanical response of tissue phantoms to nanosecond laser pulses

Francisco G. Pérez-Gutiérrez,[a] Santiago Camacho-López,[b] and Guillermo Aguilar[c,d]
[a]Universidad Autónoma de San Luis Potosí, Facultad de Ingeniería, Dr. Manuel Nava # 8, San Luis Potosí, S.L.P. C.P. 78209, México
[b]Centro de Investigación Científica y de Educación Superior de Ensenada, Departamento de Óptica, Carretera Ensenada – Tijuana 3918, Zona Playitas, Ensenada, B.C., C.P. 22860, México
[c]University of California, Riverside, Department of Mechanical Engineering, 900 University Avenue, Riverside, California 92521
[d]Centro de Investigación y Estudios Avanzados (CINVESTAV) del Instituto Politécnico Nacional, Campus Querétaro, México

Abstract. We present a time-resolved study of the interaction of nanosecond laser pulses with tissue phantoms. When a laser pulse interacts with a material, optical energy is absorbed by a combination of linear (heat generation and thermoelastic expansion) and nonlinear absorption (expanding plasma), according to both the laser light irradiance and material properties. The objective is to elucidate the contribution of linear and nonlinear optical absorption to bubble formation. Depending on the local temperatures and pressures reached, both interactions may lead to the formation of bubbles. We discuss three experimental approaches: piezoelectric sensors, time-resolved shadowgraphy, and time-resolved interferometry, to follow the formation of bubbles and measure the pressure originated by 6 ns laser pulses interacting with tissue phantoms. We studied the bubble formation and pressure transients for varying linear optical absorption and for radiant exposures above and below threshold for bubble formation. We report a rapid decay (of 2 orders of magnitude) of the laser-induced mechanical pressure measured (by time-resolved shadowgraphy) very close to the irradiation spot and beyond 1 mm from the irradiation site (by the piezoelectric sensor). Through time-resolved interferometry measurements, we determined that bubble formation can occur at marginal temperature increments as low as 3°C. [DOI: 10.1117/1.3644380]

Keywords: pulsed laser-tissue interactions; piezoelectric sensors; time-resolved shadowgraphy; time-resolved interferometry; pressure transients; linear absorption; nonlinear absorption; cavitation bubbles.

Paper 11382PR received Jul. 19, 2011; revised manuscript received Sep. 6, 2011; accepted for publication Sep. 8, 2011; published online Oct. 26, 2011.

1 Introduction

Laser-ablation of tissue with nanosecond laser pulses has been widely studied in the past and has been introduced in medical applications. The mechanisms of interaction between nanosecond laser pulses and biological tissues are very interesting in medicine because it is possible to induce ablation, cut, and tear with high precision and minimal thermal and mechanical damage to the surrounding tissue. An excellent review of pulsed laser ablation is given in Ref. 1. At low irradiance, the optical energy couples to the target material according to the material's linear absorption coefficient.[2,3] In this regime, thermal effects are dominant and if the laser pulse is shorter than the thermal and acoustic relaxation times, thermal and stress confinement conditions occur, launching a pressure wave generated by the thermoelastic expansion of the material.[4–6] In contrast, at high irradiance, it is possible to couple optical energy to materials that are otherwise transparent at low laser irradiances.[7] As the irradiance increases, the laser pulse induces material optical breakdown via multiphoton ionization seeding free electrons that serve as photon absorbers. When photons are absorbed further, more electrons are released serving as absorbers of more photons via an avalanche ionization.[1,2] This energy coupling mechanism is what is referred to as nonlinear optical absorption.

From a theorethical point of view, plasma formation is identified by the generation of a free electron density between 10^{18} and 10^{21} cm^{-3}.[1] However, from an experimental point of view, for nanosecond and picosecond laser pulses, the threshold for plasma formation is definded as the radiant exposure (or fluence) at which there is 50% probability that luminescent plasma is observed. This is readily seen in air or vacuum. In aqueous solutions and gel tissue models, however, plasma luminescence is not always seen in the visible part of the spectrum, even at high radiant exposures with nano-, pico-, and femtosecond pulses, so the threshold for plasma formation has to be experimentally determined through the observation of bubble formation.

Laser-induced bubbles are very important and deserve special attention as they are the principle on which tissue ablation, cutting, and tearing is based. Laser-induced bubbles, however, are not exclusive evidence of plasma formation as they may be formed by different mechanisms. When plasma bubbles are formed in transparent water or a gel, the violent expansion of plasma pushes the surrounding material, launching a

Address all correspondence to: Francisco G. Pérez-Gutiérrez, Universidad Autónoma de San Luis Potosí, Facultad de Ingeniería, Av. Manuel Nava No. 8-San Luis Potosí, San Luis Potosí C.P. 78209 Mexico; Tel: +52(444)8262330 ext 2115; Fax: 52(444)8262336; E-mail: francisco.perez@uaslp.mx.

1083-3668/2011/16(11)/115001/9/$25.00 © 2011 SPIE

shock wave, and an oscillating cavitation bubble results from vaporization of the material where plasma was formed. Under this scenario, thermal effects to the surrounding tissue are negligible.[1,8–11]

A second type of laser-induced bubbles is cavitation bubbles, which may be induced at moderate temperature increments (below 100°C for water) aided by tensile stresses. These bubbles are induced in aqueous solutions or gels with a high linear absorption coefficient, which therefore allow large temperature increments in very short periods of time. With a nanosecond laser pulse, the fast energy deposition creates the conditions to launch a compressive pressure wave. When this compressive wave interacts with a water or gel/air interface, it is reflected as a tensile wave.[5,12] This reflected tensile wave produces a low local pressure that reduces the temperature required to achieve the saturation point and therefore produces a phase change.

A third type of laser-induced bubbles are boiling bubbles, which form under fast light absorption, such as it happens with nanosecond laser pulses, where temperature increments are higher than the saturation temperature (above 100 °C for water) or even the spinodal limit.

The separation between cavitation and boiling bubbles is not well defined when the material is both heated and subjected to tensile stresses (stretched) at the same time. From this perspective, mechanical effects induced by nanosecond laser pulses are very interesting as both absorption regimes: linear (which induces heating) and nonlinear (which induces mechanical stresses without heating to surrounding material) can be found.

The objective of this study is to carry out a comprehensive experimental analysis of the mechanical effects that result when tissue models are irradiated with nanosecond laser pulses to elucidate the relative contribution of linear and nonlinear absorption to bubble formation. In particular, we focus on the formation of cavitation bubbles at very low temperature increments of only a few degrees Celcius and provide a feasible explanation for their formation in the context of linear and nonlinear optical absorption.

Three different experimental techniques are used for this purpose: 1. piezoelectric homemade polyvinylidene fluoride (PVDF) transducers,[13,14] 2. time-resolved imaging (TRI),[15] and 3. time-resolved Mach–Zehnder interferometry (TRIF).[16–18] The combination of the PVDF sensors and TRI systems allowed characterization of the pressure distribution in the vicinity of the laser irradiated spot within the tissue model, while TRIF allowed to measure pressure variations due entirely to the linear absorption of laser light at the irradiation volume.

2 Materials and Methods

2.1 *Tissue Models*

As tissue models, we used agar gels and water. Gels and water were used for PVDF transducers and TRI measurements, whereas only water was used for the TRIF experiments. For the experiments presented here, we used two different samples made of 0.2 and 0.4 g of agar powder per milliliter of deionized water. The samples were fabricated by pouring the dissolved agar into molds made with glass slides to yield slices of 1 to 11-mm thickness. Direct red is a red color organic dye which was mixed in the agar solution to provide the gels a high linear absorption coefficient in the green part of the spectrum. This is because hemoglobine (Hb) is a customary reference value for biomedical optics applications, especially when blood vessels or other blood-irrigated tissues are the target. The linear absorption coefficient of the agar gels and aqueous solutions we used were $\mu_a = 22$, 33, 47, and 97 cm^{-1} at $\lambda = 532$ nm. These linear absorption coefficients were determined according to the methodology described in Ref. 19.

2.2 *Laser Exposures and Laser Parameters*

Figure 1 shows the configurations under which laser exposures were carried out. Figure 1(a) shows the experimental setup for the measurements with the PVDF sensor. Figure 1(b) shows the configuration when the beam waist was positioned on the surface of the agar gel block; this configuration was useful to limit the interaction region to the highest irradiance (beam waist) only, and resembles common surface tissue ablation. Figure 1(c) shows the configuration when the beam waist was positioned 1 mm below the agar gel block surface to simulate deep vasculature and other deep sub-surface tissue target laser destruction.

The agar gel block was displaced after each laser exposure to a fresh site to avoid any disturbances by irregularities in the material due to remaining bubbles/craters from previous exposures. For experiments with water, a cuvette was glued to the sensor's aluminum case.

Laser energies per pulse used in the present study were kept below 1 mJ as higher energies tend to produce long lasting bubbles in agar gel when the laser pulse is focused.[20] The laser was focused to a beam waist $1/e^2$ radius of 2.3 μm, measured with the equivalent target plane (ETP) system (described below) and 0.5 NA.

2.3 *Piezoelectric Sensors*

PVDF is a polymer with pyroelectric and piezoelectric properties that make it suitable to measure laser-induced stresses. The shape of its signal carries information about the laser-tissue interaction. Such sensors are suitable for these measurements because of its low cost, fast time response, and high sensitivity. A pressure sensor was made using a 25 μm thick, aluminum-coated PVDF film. The sensor was connected to a digital oscilloscope through a 1 MΩ impedance to ensure proportionality of voltage to pressure.[21] The PVDF transducer sensitivity was 85 mV/MPa and the response time was measured to be 30 ns. However, one disadvantage is that pressure cannot be measured

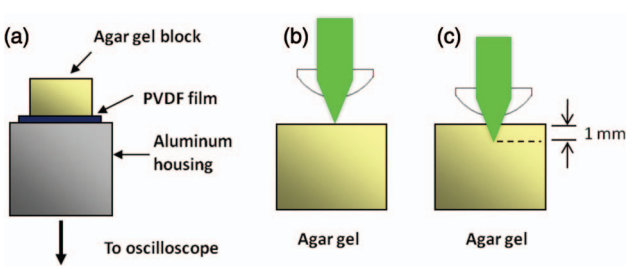

Fig. 1 (a) Experimental set-up for the measurement of pressure transients with PVDF sensors. (b) Laser exposure configuration when the beam waist was positioned on the surface of the agar gel. (c) Laser exposure configuration to simulate deep subsurface tissue targets.

closer than 1 mm to the beam focus position without risking damage to the transducer.

2.4 *TRI*

In order to overcome the limitation of PVDF sensors to measure the pressure too close to the focal point, the technique named the TRI system was developed and implemented. Images from the TRI system are useful to visualize the propagation of a shock wave because of the high refractive index change induced by the pressure difference between the shocked and ushocked regions. TRI provides information of the rate of change of the shock wave radius as a function of time, i.e., the shock wave velocity. A mathematical model (described in Sec. 3) combines the shock wave velocity, the material properties, and speed of sound, to calculate pressure difference between the shocked and unshocked regions.[15] The disadvantage of TRI is that it is not useful to measure pressure transients when plasma is not formed because the refractive index change due to acoustic waves (as opposed to shock waves) is not high enough to make the shocked–unshocked border visible.

The experimental setup for TRI of laser-agar gel interactions is shown in Fig. 2. It consists of two nanosecond laser systems electronically synchronized. The first one, used as the pump, was a 6 ns pulse duration, Q-switched, frequency doubled (λ = 532 nm) neodymium–doped yttrium aluminium garnet (Nd:YAG) laser (Brilliant, Quantel, Les Ulis Cedex, France). The second one, used as the probe, was the output of an optical parametric oscillator (OPO) which is pumped by a 6 ns pulse duration, frequency tripled ($\lambda = 355$ nm), Q-switched, Nd:YAG laser (EKSPLA, Lithuania). The probe wavelength was chosen as such because direct red dye has very low linear absorption at this wavelength and, therefore, it avoids any induced effects from the probe laser beam.

Both beams were brought colinear onto the sample by means of lenses L1 ($f = 400$ mm) and L2 ($f = 6$ mm). L2 focuses the pump beam onto the sample while L1 and L2 collimate the probe beam through the sample. The delivered energy was varied with the combination of the half wave plate and polarizer. Energy was monitored with a cross-calibrated energy meter (Ophir) to a second energy meter (Molectron, Portland, Oregon) positioned at the sample's location. The probe beam energy was varied changing the relative delay of the *Q*-switch to flash lamp by means of the triggering electronic pulse from the delay generator (DG) (BNC, San Rafael California). A magnified image of the sample is formed by the combination of lenses L3 ($f = 25$ mm) and L4 ($f = 400$ mm) onto a CCD camera (IMI Tech, Seoul, Korea). A long-pass filter with cut-off wavelength at $\lambda = 610$ nm (RF) positioned in front of the CCD blocked scattered light from the green pump beam.

The electronic DG provided the electronic pulses required to externally trigger both laser systems at 10 Hz repetition rate. Single laser pulses from the pump beam were selectively released by a mechanical shutter (MS) (Uniblitz, Rochester New York) that opens its aperture for 100 ms, therefore allowing only one laser pulse to pass through. The settings in the signal generator (SG) were 3 V, 5 Hz, 50% duty cycle. Simultaneously, the signal out of the SG was divided and also sent to trigger the CCD whose exposure time was set to 130 ms. This exposure time guaranteed that only light from the probe pulse was captured by the CCD up to tens of milliseconds after the pump pulse was released from the MS. At the same time, the SG was externally triggered with a dc power supply (Circuit Specialists, Inc., Mesa, Arizona) and a custom made hand trigger. The delay generator could produce delays as short as 1 ns, however the experimental setup time resolution was given by the probe pulse duration, which was 6 ns.

The lens L1 in the IR beam also served a second purpose. The CCD could be placed to have the pump beam retroreflected from the target onto the CCD in an image relay configuration; this setup is referred to as an ETP system. The ETP was used to set the location of the beam focus in the sample when each new sample was placed. The pump laser was focused to a beam waist $1/e^2$ radius of 2.3 μm, measured with the ETP system. The probe laser passed the sample with a $1/e^2$ radius of 175 μm and a per pulse energy of 1 μJ.

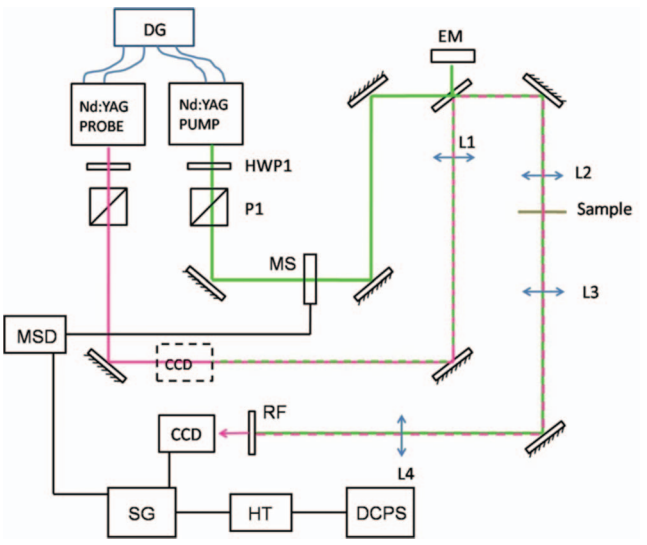

Fig. 2 Experimental set up for TRI and ETP system (see body of the text).

2.5 *TRIF*

To overcome the limitation of the TRI system to measure pressure only when shock waves are produced by plasma formation, and also to be able to measure pressure transients induced by laser fluences lower than the threshold to produce plasma, a

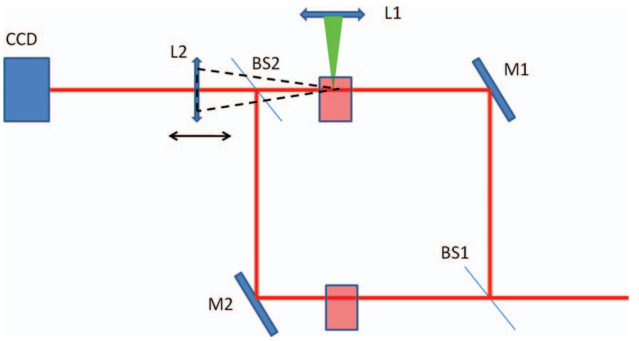

Fig. 3 Experimental set up for TRIF. Pump and probe pulses are electronically synchronized as in Fig. 2.

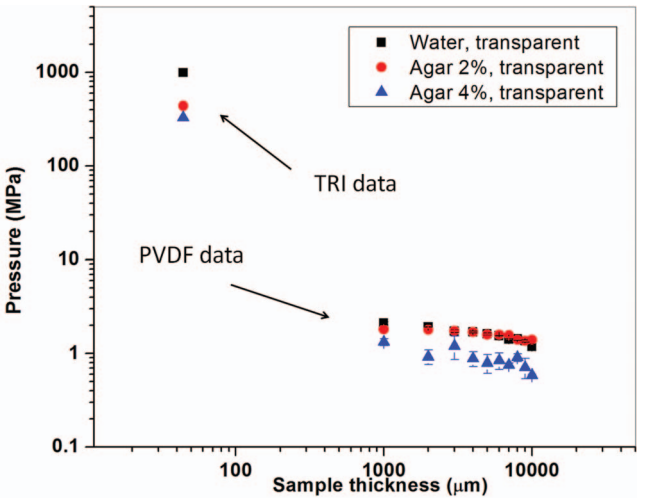

Fig. 4 Pressure distribution within agar gel from 50 μm to 10 mm measured with PVDF sensor and TRI. Energy per pulse was 500 μJ.

TRIF was built and used (Fig. 3). The probe and pump beams were electronically synchronized in the same way they were for the TRI system. The pump pulses were again delivered by the Quantel laser at $\lambda = 532$ nm, although in this case the probe pulses were delivered at $\lambda = 633$ nm by the OPO of the EKSPLA laser system. The pump pulse was focused in the bulk of the direct red solution by a removable aspheric lens L1. The probe pulse was split into two paths by means of a 50/50 beam splitter (BS1). A quartz cuvette filled with an aqueous solution of direct red was conveniently placed so that the pump pulse was incident on it from above and its energy absorbed by the direct red solution. Another quartz cuvette filled with the same direct red solution was positioned in the reference arm of the interferometer so that both optical paths were equal. The two arms were recombined at a second 50/50 beam splitter (BS2) where an interference fringe pattern was generated. A 50 mm focal length lens (L2) magnified the interferogram and sent the image to the CCD camera. As in the TRI system, the temporal resolution of the TRIF system was given by the probe pulse duration.

3 Results

3.1 *Pressure as a Function of Sample Thickness*

Figure 4 shows the pressure distribution inside the agar gel blocks and deionized water for sample thicknesses ranging from 50 μm to 10 mm. Pressure waves were measured using PVDF sensors and TRI. PVDF data were obtained using agar samples of different thicknesses, which allows one to measure pressure at specific distances from the beam waist. The energy per pulse was 500 ± 50 μJ. The pressure amplitude for the 2% agar blocks and deionized water overlap and show a linear decay with sample thickness; the pressure amplitude drops by 25% within the sample thickness range (1 to 10 mm). In contrast, the maximum pressure amplitude for the 4% agar gel blocks is approximately 40% lower than that for 2% agar blocks and water for practically all sample thicknesses.

The shock wave amplitude was investigated indirectly using a phenomenological model that involves the information that can be directly obtained from TRI. Such information is the shock wave velocity which is obtained by measuring the radius of the shockwave front as a function of the relative delay from the pump and probe pulses. A mathematical derivation of this model which relates the shock wave velocity to the particle velocity is explained in Ref. 15 and used herein:

$$P_1 - P_2 = \rho_2 U \left(\frac{U - C_s}{S} \right), \tag{1}$$

where P_1-P_2 is the pressure difference between the shocked and unshocked regions, ρ_2 is the agar gel density, U is the shock wave velocity, C_s is the speed of sound, and S is the Hugoniot coefficient for gel. C_s and S values are obtained from Ref. 15 and are 1520 m/s and 2.0, respectively.

3.2 *Pressure for Surface and Deep Subsurface Tissue Targets*

Figure 5(a) shows the pressure wave originated when an unfocused nanosecond laser pulse is incident on an absorbing agar gel block. The leading edge of the positive peak is the region containing the absorption information of the sample. The peak indicates the acoustic wave amplitude initially induced by the laser pulse at the surface of the sample. If stress confinement

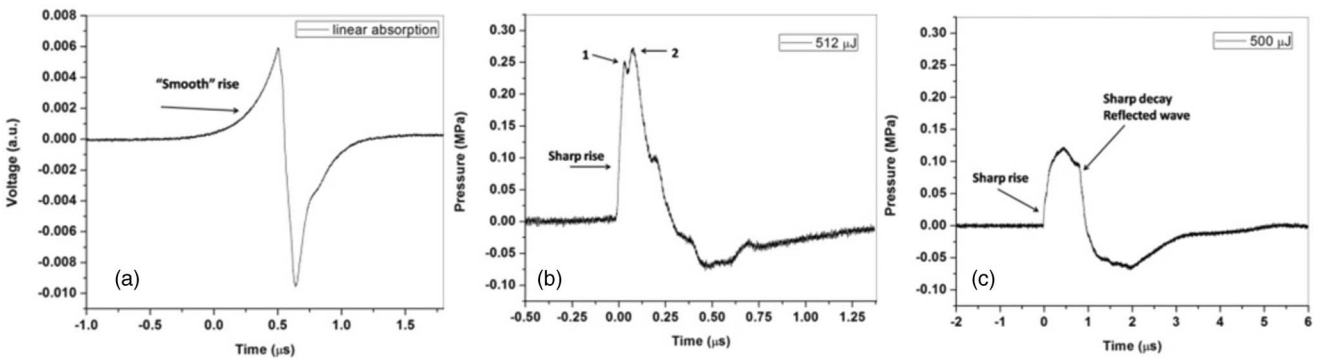

Fig. 5 (a) Pressure signal obtained with a PVDF sensor when an unfocused, 6 ns laser pulse is incident on an absorbing, 10-mm thick agar gel. $\mu_a = 33$ cm^{-1}. (b) Pressure signal obtained with PVDF sensor when a focused, 6 ns laser pulse is incident on an absorbing 10 mm thick agar gel. Beam waist was positioned on the surface of the agar gel. $\mu_a = 33$ cm^{-1}. (c) Pressure signal obtained with PVDF sensor. Focused 6 ns laser pulse is incident on absorbing, 10 mm thick agar gel. The beam waist was positioned 1 mm below the agar gel surface. $\mu_a = 33$ cm^{-1}.

conditions are met and ablation threshold is not overcome, the entire signal has a symmetric bipolar shape such that the integral vanishes.[6] Figure 5(b) shows the typical signal when the beam waist is positioned on the gel surface and Fig. 5(c) corresponds to the configuration positioning the beam waist 1 mm below the gel surface, to simulate a deep sub-surface tissue target. All these signals show a sharp increase at $t = 0$, followed by a maximum and a minimum.

3.3 *Linear Absorption Coefficient*

Figure 6 shows the amplitude of the pressure signals for different linear absorption coefficients as a function of energy (per pulse), detected with the PVDF sensor when the laser beam waist was positioned 1 mm below the 2% agar gel surface and 10 mm away from the sensor. The transparent agar gel shows higher pressure increments because almost the entire energy from the laser pulse is deposited in the focal volume and is readily available to produce plasma. In contrast, pressure amplitude for absorbing agar gels show lower pressure increments because the beam propagates 1 mm through the gel and the energy that remains to produce plasma is less than in the previous case.

3.4 *TRIF*

Figure 7 shows images of a cavitation bubble that was formed when the pump laser beam was focused in the bulk of the direct red water solution and the laser irradiance at the focal point was not high enough to produce plasma. No fringe shift was observed, most likely due to the tiny size (in the order of a single fringe) of the produced bubble.

Given that no change in the interferogram was registered when the laser beam was focused in the direct red solution with laser fluence under the threshold for plasma formation, the approach was to increase the size of the laser beam and laser pulse energy to create cavitation bubbles under similar conditions of pump fluence. Figure 8 shows a schematic of the new experimental conditions. For these experiments, lens L1

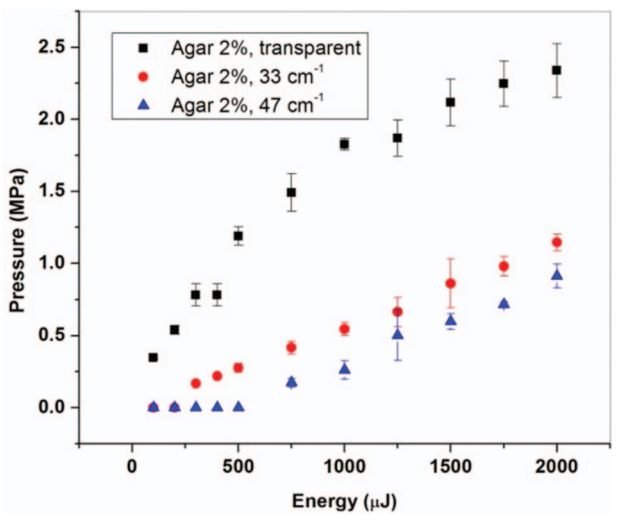

Fig. 6 Pressure amplitude as a function of per pulse energy. Laser pulses were focused 1 mm below the surface of agar gel blocks.

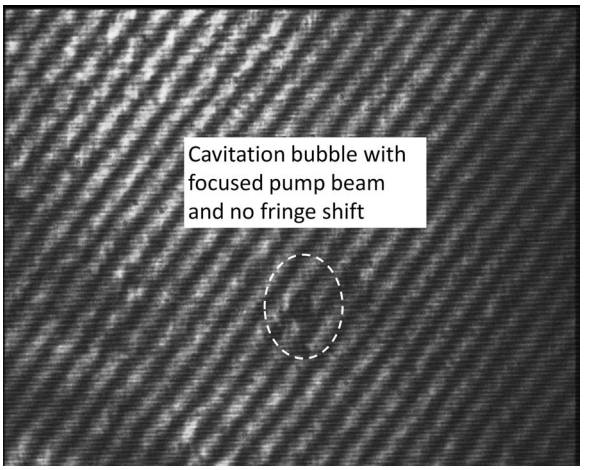

Fig. 7 TRIF image of a cavitation bubble when a nanosecond laser pulse focused in the bulk of a direct red solution did not have enough irradiance to produce plasma. No phase shift was observed.

in Fig. 3 was removed; the pump beam was collimated and reduced to 1-mm diameter. The absorption coefficient of the sample was $\mu_a = 22\ \mathrm{cm}^{-1}$ which is equivalent to a penetration depth $\delta = 450\ \mu$m. Under such conditions, δ is comparable to the beam diameter and a cylindrical wave propagating in the radial direction results.

Figure 9 shows images of TRIF carried out in the irradiated volume. Although better appreciated in the video recording, these set of images show the cylindrical wave propagation; as a slight fringe shift along the beam propagation path. Note, however, that only a minimal phase change was observed as a function of time. This is because the heat generated upon laser pulse energy absorption is confined to the irradiation volume for at least the 5 μs delay with respect to the pump pulse when the images were taken.

Despite the slight phase change observed in Fig. 9, Fig. 10 shows that multiple microcavitation bubbles were formed in the bulk of a direct red aqueous solution, for which the absorption coefficient was $\mu_a = 22\ \mathrm{cm}^{-1}$ and the energy per pulse was 6 mJ. Figure 10(a) shows the region of interest before the pump

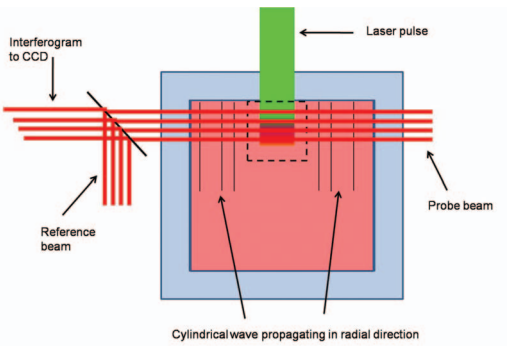

Fig. 8 Experimental conditions in which a nanosecond laser pulse is linearly absorbed in an aqueous solution of direct red, and the interaction region is observed through TRIF. Because δ is comparable to the beam diameter, a cylindrical wave propagating in the radial direction results.

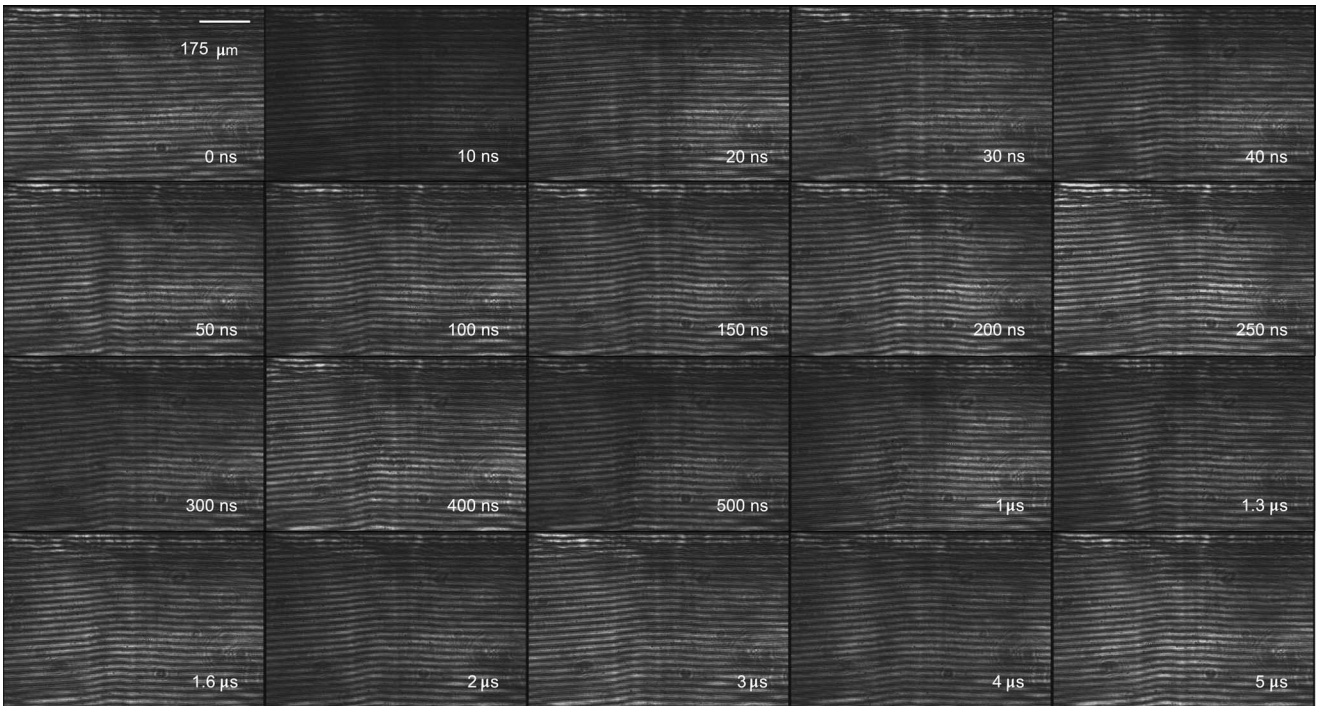

Fig. 9 TRIF images when a collimated nanosecond laser pulse was incident on a quartz cuvette filled with direct red solution. Laser spot size was 1 mm. No significant difference in the phase change was observed as a function of time.

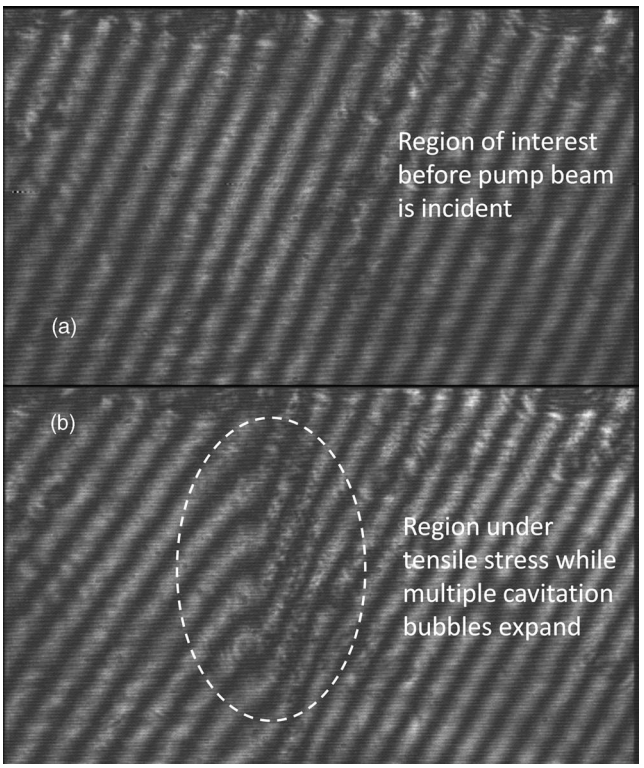

Fig. 10 (a) Region of interest before the pump laser pulse was incident onto the absorbing solution. (b) Cavitation bubbles formed in the bulk of a direct red solution with $\mu_a = 22\ \mathrm{cm}^{-1}$. Energy per pulse was 6 mJ and laser spot size 1 mm; time delay with respect to pump pulse was 500 ns. Under such conditions, the maximum calculated temperature increment was $\sim 3\,^{\circ}\mathrm{C}$. Arrows point to cavitation bubble formation.

pulse is incident onto the absorbing solution; Fig. 10(b) shows an image of cavitation bubble formation within the same region 500 ns after the pump pulse was triggered.

4 Discussion

4.1 *Pressure/Shock Waves*

The results presented in Fig. 4 show the 3 orders of magnitude difference between the pressure amplitude of a shock wave near to (50 μm) and several millimeters (1 to 10 mm) away from the focal point. It is expected that the shock wave becomes a pressure wave propagating at sonic speed in less than 150 ns after optical breakdown.[8]

In contrast to Fig. 5(a) that shows the pressure wave originated when an unfocused nanosecond laser pulse is incident on an absorbing agar gel block, the sharp rise in Figs. 5(b) and 5(c) is produced by a shock wave that is launched due to plasma formation.

The pressure signal in Fig. 5(b) shows two spikes. The first, labeled number 1, is generated by the plasma formation in air and propagates downwards to the sensor. The second spike, labeled number 2, is originated by linear absorption of the light that propagates after the plasma-originated wave and is incident on the agar gel surface. The final signal shown in Fig. 5(b) is the superposition of these two waves. Interestingly, oscilloscope traces with spikes very similar to those obtained here are shown in recent studies where a PDVF sensor was developed to monitor nanosecond laser induced-bubble collapse near a solid surface.[16,17] Clearly, the laser exposure configuration used in the present study is different and bubble collapse is not the mechanism responsible for the spikes we observe in our experiments.

Figure 5(c) shows that the lower part of the spherical shock wave propagates as a compressive wave toward the sensor, while the upper part propagates also as a compressive wave toward the free surface and is reflected backwards with an inverted sign as a tensile wave. The change from compressive to tensile wave takes place due to the acoustic impedance mismatch between the agar gel surface and air. The tensile wave is clearly shown as a sharp decay in the pressure wave in Fig. 5(c). The time difference between the rise edge of the pulse (compressive) and the fall edge (tensile), as shown in Fig. 5(b), agrees well with the time that it takes for an acoustic wave to travel 2 mm at 1500 m/s. For this rough calculation, the deceleration of the wave from shock wave to a pressure wave is neglected.

Previous studies[22,23] report experimental and numerical calculations of nanosecond laser pulse-induced shock waves on tissue phantoms that exhibit a compressive peak followed by a low-amplitude tensile component. The tissue phantoms used in one of those studies[23] were polyacrylamide (PAA) gels with varying elastic modulus and water. The authors use PAA gels because they are a more realistic tissue phantom compared to water, they emphasize the existence of the tensile component in PAA gels because real tissue is much more susceptible to tensile stress than to compressive stress, while they did not observe the tensile component in water. In our experiments with linearly absorbing agar gels focusing the beam on the sample surface [Fig. 5(b)] and water (results not shown), we observed the same behavior when laser irradiance was high enough for plasma formation, meaning that optical breakdown is the dominant mechanism of interaction despite the linear absorption in our gels.

When using a piezoelectric sensor to measure the pressure induced in agar gels as the linear absorption coefficient was increased, as it is shown in Fig. 6, no signal was detected when lower than 500 μJ laser pulses were focused 1 mm underneath the surface, for the 10-mm thick agar gel blocks with 47 cm^{-1}. This is because the heat generated while the beam propagates through 1 mm is too low to induce a sufficiently large thermoelastic expansion of the heated material to launch a pressure wave detectable by the sensor located 9 mm underneath the focus. No changes of the pressue signal as a function of the pulse energy were detected for the configuration when the beam waist was positioned on the surface of the agar gel.

4.2 *Bubble Formation*

The TRIF experiments reported in Fig. 7 show the existence of a small bubble at or near the focal point of the laser. However, the lack of fringe shift in the interferogram is because the beam waist at that location was about 6 μm in diameter, which is too slender to induce a significant phase change in the optical propagation path of the probe arm with respect to the reference arm of the Mach–Zehnder interferometer.

This situation was corrected by expanding the beam and increasing the laser pulse energy. New experiments showed a more obvious presence of bubbles (Fig. 9) and a mild fringe shift. Interestingly, a simple calculation of thermal confinement showed that the temperature increment associated with the irradiation conditions was of only about 3 °C, which is too low to induce a phase change at standard pressure (described in the next paragraph). At the same time, however, this led the research to pay attention to similar scenarios studied before where the combined influence of tensile stresses and mild temperature increments explained the formation of cavitation bubbles.

Assuming thermal confinement and no phase change, the temperature increment associated with these irradiation conditions was calculated according to:

$$\Delta T = \frac{\mu_a F}{\rho c_p}, \tag{2}$$

where ΔT is temperature increment, μ_a is absorption coefficient (22 cm^{-1}), F is laser pulse fluence (0.63 J/cm^2), ρ is density (1000 kg/m^3), and c_p is specific heat (4186 $J/kg \cdot K$), resulting in ~3 °C, which is too low to induce a phase change at standard pressure. The influence of tensile stresses on the phase change is evident at such a low temperature increment under this perspective.

The fringe pattern shape can be approximated as a triangular profile according to Fig. 11. The maximum refractive index change can be calculated using Eq. (3) following the procedure in Ref. 17 if the phase change is known from the interferogram

$$\delta n_{\max} = \frac{\lambda_{\text{int}} \cdot \delta\Phi_{\max} \cdot 1.5}{2\pi \cdot 2\sqrt{R^2 - x_m^2}}, \tag{3}$$

where $\delta n_{\max}$ is the maximum refractive index change, λ_{int} is the wavelength of the interferogram, $\delta\Phi_{\max}$ is the maximum phase change, and R and x_m can be measured from the interferogram in Fig. 11, which showed the following values: $\lambda_{\text{int}} = 28$ μm, $\delta\Phi = \pi$, $R = 1104$ μm, and $x_m = 540$ μm. The resulting refractive index change with this information is $\delta n_{\max} = 0.01090$.

An empirical equation that relates the refractive index of water as a function of pressure, temperature, and light wavelength was reported in Ref. 24. For the case studied here, considering the temperature increment of 3 °C, and the 633 nm wavelength of the probe pulse, the mentioned equation reduces to Eq. (4):

$$0 = \delta n + 1.48\times10^{-5}\delta p - 1.89\times10^{-9}\delta p^2, \tag{4}$$

where δn is the refractive index change and δp is pressure change in bars. Solving for δp with the refractive index change δn calculated above results in a negative pressure change (decrement). Such pressure with negative sign is a tensile wave, which

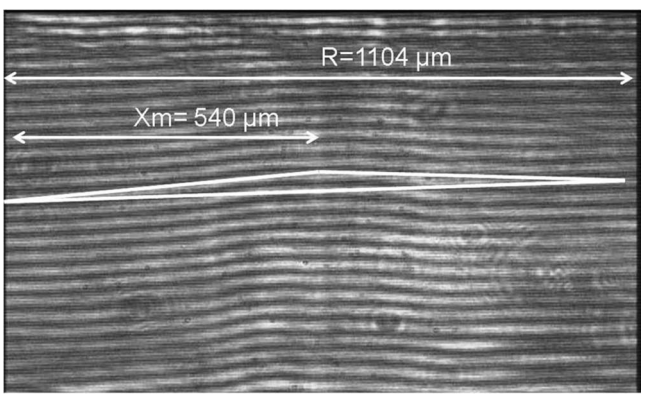

Fig. 11 Fringe shape can be approximated as a triangle. Using Eq. (3) and measuring the distances x_m and R, the maximum refractive index change can be calculated.

explains caviation bubble formation with such a low temperature increment.

In previous studies, microcavitation bubbles were created in an aqueous solution of potassium chromate by a nanosecond laser pulse for temperature increments as low as 5 °C.[5,12] In those experiments, the laser spot size was much larger than the light penetration depth and, therefore, the compressive pressure wave that resulted from fast thermoelastic expansion of the irradiated volume surrounded by cold material was a plane wave. Such wave propagates in both directions, the optical path direction and in the opposite direction toward the solution/air interface. When the latter wave reaches the solution/air interface, it encounters an acoustic mismatch because of the lower acoustic impedance of air compared with that of water, and is reflected as a tensile wave. The combination of the tensile wave and moderate temperature increments is the mechanism responsible for initiating the cavitation bubbles.

In the experiments presented here, the laser spot size is comparable with the light penetration depth, so the resulting wave from the thermoelastic expansion was a cylindrical wave. Thus, the expansion in the radial direction stretches the irradiated volume and originates tensile stresses within the interaction volume. The expansion of the irradiated volume in the optical path direction also takes place, but the radial expansion is more important. Indeed, the plane wave in the optical path was not even detected with TRIF. Therefore, what really happens is that the cylindrical irradiated volume is being stretched in the radial direction due to the thermoelastic expansion, such that the local pressure in the center of the cylinder is low enough to induce microcavitation bubbles aided by a low temperature increment, also of about 3 to 5 °C. Pre-existing microbubbles and impurities may serve as nucleation centers that facilitate cavitation.

5 Conclusions

Mechanical effects of irradiation with nanosecond laser pulses of agar gels were studied with three experimental techniques: PVDF sensors, TRI, and TRIF. It was found through a PVDF sensor that the amplitude of the pressure waves for samples between 1 and 10 mm thick has no significant difference for the agar gel concentrations tested. However, the pressure amplitudes measured a few tens of micrometers away from the beam waist are 2 orders of magnitude higher than 1 mm away; in other words, the pressure amplitude decreases 2 orders of magnitude in the first millimiter of propagation. Increasing the linear absorption coefficient of the samples decreases the amplitude of the pressure wave when the beam was positioned 1 mm below the surface; this is so because plasma formation is weaker due to the exponential decay of energy given by the linear absorption and light propagation. This is a clear indication that plasma formation is the dominant interaction mechanism in these experiments; an important application of this result is in ablation of deep vasculature or other tissue targets located deep into skin. Our TRIF results revealed the importance of tensile stresses on the formation of microcavitation bubbles when very low temperature increments (∼3 °C) take place upon laser energy linear absorption. It must be noted that the experimental approaches presented throughout this paper allow to clearly discriminatee between plasma-produced bubbles, which require high irradiances and cavitation-produced bubbles, produced at modest irradiances and low optical absorption.

Acknowledgments

FGPG acknowledges financial support form UC MEXUS-CONACyT fellowship for graduate studies, 2009 UC MEXUS Dissertation Research Grant, and UCR Chancellor's Dissertation Fellowship Award. SCL acknowledges CONACyT Grant No. 57309. Also, we thank Mr. Edgar Arturo Chávez Urbiola for his help with some experiments. We also appreciate assistance from Dr. Francisco Oviedo Tolentino and María Luisa López de Lara González preparing the figures for this article.

References

1. A. Vogel and V. Venugopalan, "Mechanisms of pulsed laser ablation of biological tissues," *Chem. Rev.* **103**(2), 577–644 (2003).
2. M. Niemz, *Laser-Tissue Interactions: Fundamentals and Applications*, Springer, New York (2002).
3. A. J. Welch and M. J. C. v. Gemert, *Optical-Thermal Response of Laser-Irradiated Tissue*, Plenum Press, New York (1995).
4. A. A. Oraevsky, "Laser-induced acoustic and shock waves in ocular tissues," Armstrong Laboratory, Occupational and Environmental Health Directorate, Optical Radiation Division (1995).
5. A. A. Oraevsky, S. L. Jacques, R. O. Esenaliev, and T. F. K., "Pulsed laser ablation of soft tissues, gels, and aqueous solutions at temperatures below 100 °C," *Lasers Surg. Med.* **18**(3), 231–240 (1996).
6. G. Paltauf and P. E. Dyer, "Photomechanical processes and effects in ablation," *Chem. Rev.* **103**(2), 487–518 (2003).
7. R. W. Boyd, *Nonlinear Optics*, Academic Press, Oxford (2008).
8. A. Vogel, S. Busch, and U. Parlitz, "Shock wave emission and cavitation bubble generation by picosecond and nanosecond optical breakdown in water," *J. Acoust. Soc. Am.* **100**(1), 148–165 (1996).
9. A. Vogel and W. Lauterborn, "Acoustic transient generation by laser-produced cavitation bubbles near solid boundaries," *J. Acoust. Soc. Am.* **82**(2), 719–731 (1988).
10. A. Vogel, W. Lauterborn, and R. Timm, "Optical and acoustic investigations of the dynamics of laser-produced cavitation bubbles near a solid boundary," *J. Fluid Mech.* **206**, 299–338 (1989).
11. A. Vogel, K. Nahen, D. Theisen, and J. Noack, "Plasma formation in water by picosecond and nanosecond Nd:YAG laser pulses-Part I: Optical breakdown at threshold and superthreshold irradiance," *IEEE J. Sel. Top. Quantum Electron.* **2**(4), 847–860 (1996).
12. A. A. Oraevsky, S. L. Jacques, and F. K. Tittel, "Mechanism of laser ablation for aqueous media irradiated under confined-stress conditions," *J. Appl. Phys.* **78**(2), 1281–1290 (1995).
13. Y. C. Wang and Y. W. Chen, "Application of piezoelectric PVDF film to the measurement of impulsive forces generated by cavitation bubble collapse near a solid boundary," *Exp. Therm. Fluid Sci.* **32**, 403–414 (2007).
14. Y. C. Wang, C. H. Huang, Y. C. Lee, and H. H. Tsai, "Development of a PVDF sensor array for measurement of the impulsive pressure generated by cavitation bubble collapse," *Exp. Fluids* **41**, 365–376 (2006).
15. R. Evans, S. Camacho-López, F. G. Pérez-Gutiérrez, and G. Aguilar, "Pump-probe imaging of nanosecond laser-induced bubbles in agar gel," *Opt. Express.* **16**(10), 7481–7492 (2008).
16. B. Kim, M. D. Feit, A. M. Rubenchick, E. J. Joslin, P. M. Celliers, J. Eichler, and L. B. Da Silva, "Influence of pulse duration on ultrashort laser pulse ablation of biological tissues," *J. Biomed. Opt.* **6**(3), 332–338 (2001).
17. B. Kim, A. M. Komashko, A. M. Rubenchick, M. D. Feit, S. Reidt, L. B. Da Silva, and J. Eichler, "Interferometric analysis of ultrashort pulse laser-induced pressure waves in water," *J. Appl. Phys.* **94**(1), 709–715 (2003).
18. L. Martí-López, R. Ocaña, J. A. Porro, M. Morales, and J. L. Ocaña, "Optical observation of shock waves and cavitation bubbles in high intensity laser-induced shock processes," *Appl. Opt.* **48**, 3671–2380 (2009).

19. J. A. Viator, S. L. Jacques, and S. Prahl, "Depth profiling of absorbing soft materials using photoacoustic models," *IEEE J. Sel. Top. Quantum Electron.* **5**(4), 989–996 (1999).
20. F. G. Pérez-Gutiérrez, R. Evans, S. Camacho-López, and G. Aguilar, "Short and ultrashort laser pulse induced bubbles on transparent and scattering tissue models," *Proc. SPIE* **6435**, 64350V (2007).
21. M. A. P. Giao, N. A. S. Redrigues, R. Riva, and C. Schwab, "PVDF sensor in laser ablation experiments," *Rev. Sci. Instrum.* **75**, 5213–5215 (2004).
22. E. A. Brujan, "Dynamics of shock waves and cavitation bubbles in bilinear elastic-plastic media, and the implications to short-pulsed laser surgery," *Eur. Phys. J. Appl. Phys.* **29**, 115–123 (2005).
23. E. A. Brujan and A. Vogel, "Stress wave emission and cavitation bubble dynamics by nanosecond optical breakdown in a tissue phantom," *J. Fluid Mech.* **558**, 281–308 (2006).
24. I. Thormahlen, J. Straub, and U. Grugull, "Refractive index of water its dependence on wavelength, temperature, and density," *J. Phys. Chem. Ref Data* **14**, 933–945 (1985).